Targeting the Platelet-Derived Growth Factor-beta Stimulatory Circuitry to Control Retinoblastoma Seeds

Zachary K. Goldsmith,[1] William Coppess,[1] Andrew S. Irvine,[1] Kelley Yuan,[1] Samuel R. Barsh,[1] Madison K. Ritter,[1,2] Matthew W. McEwen,[1] Jacqueline Flores-Otero,[3,4] Aileen Garcia-Vargas,[4,5] Magaly Martinez-Ferrer,[4,6] Rachel C. Brennan,[1,7] Vanessa M. Morales-Tirado,[1,8] and Matthew W. Wilson[1,9]

[1]Department of Ophthalmology, Hamilton Eye Institute, University of Tennessee Health Science Center, Memphis, Tennessee, United States
[2]Department of Biology, Furman University, Greenville, South Carolina, United States
[3]Department of Anatomy and Neurobiology, University of Puerto Rico School of Medicine, San Juan, Puerto Rico, United States
[4]University of Puerto Rico Comprehensive Cancer Center, San Juan, Puerto Rico, United States
[5]Department of Pharmacology and Toxicology, University of Puerto Rico School of Medicine, San Juan, Puerto Rico, United States
[6]Department of Pharmaceutical Sciences, University of Puerto Rico School of Pharmacy, San Juan, Puerto Rico, United States
[7]Department of Oncology, St. Jude Children's Research Hospital, Memphis, Tennessee, United States
[8]Department of Microbiology, Immunology, and Biochemistry, University of Tennessee Health Science Center, Memphis, Tennessee, United States
[9]Department of Surgery, St. Jude Children's Research Hospital, Memphis, Tennessee, United States

PURPOSE. Vitreous seeding remains the primary reason for treatment failure in eyes with retinoblastoma (Rb). Systemic and intra-arterial chemotherapy, each with its own inherent set of complications, have improved salvage rates for eyes with advanced disease, but the location and biology of vitreous seeds present a fundamental challenge in developing treatments with minimal toxicity and risk. The aim of this study was to target the platelet-derived growth factor (PDGF)– PDGF-receptor β (PDGFRβ) signaling pathway and investigate its role in the growth of Rb seeds, apoptotic activity, and invasive potential.

METHODS. We performed ex vivo analyses on vitreous samples from Rb patients that underwent enucleation and from patient-derived xenografts. These samples were evaluated by quantitative PCR, immunohistochemistry, and ELISA. The effects of disruption of the PDGF-PDGFRβ signaling pathway, both by pharmacologic and genomic knockdown approaches, were evaluated in vitro by cell proliferation and apoptotic assays, quantitative PCR analyses, Western blotting, flow cytometry, and imaging flow cytometry. A three-dimensional cell culture system was generated for in-depth study of Rb seeds.

RESULTS. Our results demonstrated that PDGFRβ signaling is active in the vitreous of Rb patients and patient-derived xenografts, sustaining growth and survival in an AKT-, MDM2-, and NF-κB-dependent manner. The novel three-dimensional cell culture system mimics Rb seeds, as the in vitro generated spheroids have similar morphologic features to Rb seeds and mimicked their natural physiology.

CONCLUSIONS. Targeting the PDGFRβ pathway in vitro reduces Rb cell growth, survival, and invasiveness and could augment current therapies. This represents a novel signaling pathway for potential targeted therapy to further improve ocular survival in advanced Rb.

Keywords: retinoblastoma, PDGF, vitreous seeds, imatinib, molecular medicine

The greatest challenge in treatment of retinoblastoma (Rb) is the recurrence or resistance of vitreous seeding to current therapies. Overall, patients that have vitreous seeding have a poorer prognosis for ocular salvage.[1–6] Although the mechanism controlling refractory or recurrent vitreous disease is unclear, it is likely related to a unique property of Rb cells that allows them to adapt and propagate in semisolid or liquid microenvironments, such as the vitreous and subretinal compartments.[7]

Understanding the tumor microenvironment is an important step in achieving overall treatment goals for Rb, including patient survival, globe salvage, and vision preservation.[6,8] The vitreous body is a translucent medium in the eye composed of liquid (99%) and solid (1%) phases. Recent research has identified the presence of some inflammatory, mitogenic, and immunosuppressive mediators in the vitreous[9–11] capable of promoting homeostasis as well as pathologic processes, most notably diabetic retinopathy and proliferative vitreous retinopathy resulting from complex rhegmatogenous retinal detachments.[10,12–14] Platelet-derived growth factor (PDGF) has been identified as one such key regulator.[13,15] Based on this evidence, we hypothesize that cellular infiltrates secrete PDGF

in the vitreous, which may provide mitogenic activity to Rb cells via the PDGF-receptor (PDGFR).[16–20] We found that reducing PDGFRβ signaling in Rb tumor cells in vitro reduces growth, cell survival, and invasion potential via the AKT, MDM2, and NF-κB signaling pathways.

METHODS

Ethics Approval and Consent to Participate

The institutional review board at SJCRH and The University of Tennessee Health Science Center (UTHSC) approved all experiments involving human subjects. Informed consent was obtained cases where vitreous was harvested at the time of enucleation, an optional research objective that is part of an on-going prospective clinical trial (ClinicalTrials.gov, NCT01783535). This is in full compliance with and adheres to the tenets of the Declaration of Helsinki. The Institutional Animal Care and Use Committee at SJCRH approved all animal experiments. All protocols followed the ARVO Statement for the Use of Animals in Ophthalmic and Vision Research, in addition to the guidelines for laboratory animal experiments.

Cell Lines

Y79[21] (ATCC HTB-18) and Weri-Rb-1[22] (ATCC HTB-169) cell line information and culture media were previously described.[23]

Vitreous Samples

Eyes were trephined after enucleation without disruption of underlying structures, which is important for diagnostic and staging purposes. Vitreous was aspirated using an 18-gauge needle and a 3-mL syringe. Vitreous from healthy controls were purchased from BioreclamationIVT (Baltimore, MD, USA).

Reagents

Gleevec was purchased in its generic chemical form, imatinib mesylate (IM; PubChem ID, 123596), from Sigma-Aldrich (Saint Louis, MO, USA). Lyophilized reagent was dissolved in deionized, distilled water to 10 mM and stored at −20°C. Lyophilized recombinant human PDGF-BB (10 μg) was purchased from Thermo Scientific (Waltham, MA, USA), dissolved in 1 mL 100 mM acetic acid with 0.1% BSA, and stored at −20°C.

Immunohistochemistry

Enucleated eyes from Rb patients treated at St. Jude Children's Research Hospital (SJCRH) were fixed, paraffin-embedded, and serially sectioned. The probes antihuman PDGFRβ (16868; Abcam, Cambridge, MA, USA) and antihuman p-PDGFRβ (sc-339; Santa Cruz Biotechnology, Inc., Dallas, TX, USA) were used. Patient-derived orthotopic xenografts (PDX) for Rb were described before.[24] Briefly, tumor was harvested from the eyes of patients primarily enucleated for Rb. The samples were taken from a diverse patient population, with respect to clinical presentation, sex, and race. Samples were dissociated with trypsin, collected, and resuspended in a solution of RPMI and 10% fetal calf serum at 10,000 cells/μL. Approximately 50,000 cells were injected into the eyes of SCID (NOD.CB17-Prkdc[scid]/J) mice.

MTS Cell Proliferation Assay

Cell proliferation was investigated using the CellTiter96 AQueous One Solution Cell Proliferation Assay reagent (Promega, Madison, WI, USA), as described before[23] by plating Y79 cells at a density of 5.0×10^3 cells per well.

Protein Assays

PDGF-AB/PDGF-BB/VEGF ELISA. Vitreous samples were diluted 1:10 with assay buffer from the respective Invitrogen Human PDGF ELISA Kit (Thermo Scientific). Diluted samples were placed in an antibody-coated microwell plate along with appropriate standards following manufacturer's protocols. Absorbance calculated using both 450 nm and 550 nm as reading wavelengths. Assays were conducted in triplicates.

Cleaved Caspase-3 ELISA. A caspase-3 (active) ELISA kit (Thermo Scientific) was used according to manufacturer's instructions: 30 μg of total extracted protein was incubated in a microplate well in triplicate at room temperature (RT) for 2 hours. Absorbance values were calculated as above.

Western Blot Analyses. We followed our published protocols[25,26] for electrophoresis. Membranes were blocked with 5% BSA in Pierce Tris Buffered Saline Tween-20 for 1 hour, followed by incubation with primary antibodies overnight at 4°C. HRP-linked secondary antibodies were added and incubated at RT for 1 hour. Signal was detected using SuperSignal West Pico Chemiluminescent Substrate (Thermo Scientific). The endogenous control was either β-ACTIN or GAPDH (both from Cell Signaling Technology [CST], Beverly, MA, USA). Experiments were conducted in triplicate. The primary antibodies were anti-PDGFRβ (sc-432; 1:100), anti-phosphorylated PDGFRβ (sc-373805; 1:100), anti-VEGF (sc-53462; 1:200), anti-Flk-1 (also known as [aka] VEGFR2, sc-6251; 1:200), anti-p-Flk-1 (aka p-VEGFR2, sc-101821; 1:100), anti-MDM2 (sc-965; 1:200), antiphosphorylated MDM2 (sc-53368; 1:200), anti-AKT (catalog no. 9272; CST; 1:1000), antiphosphorylated AKT (catalog no. 4058; CST; 1:1000), anti-BCL-2 (catalog no. 2870; CST; 1:1000), anti-GAPDH (catalog no. 8884; CST; 1:1000). Secondary antibodies were anti-mouse IgG HRP-linked (catalog no. 7076; CST; 1:1000) and anti-rabbit IgG HRP-linked antibodies (catalog no. 7074; CST; 1:1000).

Flow Cytometry Studies

Apoptosis. Annexin-V and propidium iodide (PI) were used as before.[27] Data were acquired using a BD LSR II Cytometer (BD Biosciences, San Jose, CA, USA) with BD FACSDiva software; analysis was performed using FlowJo v.X.0.0.8 (FlowJo, LLC, Tree Star, Ashland, OR, USA). Samples were analyzed in triplicate.

PDGFRβ Expression. Y79 Rb cells were labeled with anti-PDGFRβ (sc-432; 1:50) on ice for 30 minutes, followed by incubation with a donkey anti-rabbit Alexa Fluor 647 (Thermo Scientific; 1:50) secondary antibody for 30 minutes. Cells were fixed with 2% paraformaldehyde for 20 minutes prior to analysis. Analyses of PDGFRβ from three-dimensional (3D) assays were conducted as follows: spheroids were transferred to a fluorescence-activated cell sorting (FACS) tube by using a magnetic pen, followed by spheroid disruption by pipetting. Cells were labeled as above. Controls included an isotype control and unlabeled samples. Single label controls were set up using The AbC Total Antibody Compensation Bead Kit (Thermo Scientific). Data acquisition was done in a ZE5 Cell Analyzer from Propel Labs (Fort Collins, CO, USA). Analysis was done as above.

p65 NF-κB Nuclear Translocation by Imaging Flow Cytometry. Collected cells were fixed in 2% paraformaldehyde and permeabilized in 0.01% Triton X-100. Samples were blocked with PBS/1% fetal bovine serum before addition of anti-p65 (catalog no. 8242; CST; 1:100) antibody for 1 hour on ice. Cells were washed with PBS, and donkey anti-rabbit Alexa

Fluor 488 (Thermo Scientific; 1:100) secondary antibody was added for 1 hour. Nuclei were labeled with DRAQ5 (BioLegend, San Diego, CA, USA; 1:100). Cells were analyzed using the Amnis FlowSight Imaging Cytometer (EMD Millipore, Seattle, WA, USA). Data were analyzed using IDEAS software (EMD Millipore). Mean fluorescent intensity (MFI) was measured to investigate levels of p65 as well as the percentage of cells with p65 translocation to the nucleus. The fluorescence controls were single labeled cells acquired with both 488 nm and 642 nm. We collected a minimum of 10,000 events (cells) from each sample, and experiments were done in triplicate.

Cell Invasion Assay. A CytoSelect 24-well cell invasion kit (Cell BioLabs, Inc., San Diego, CA, USA) was used to measure invasion of Y79 cells as described previously.[26]

3D Cell Culture System. Y79 cells (5.0×10^6 cells per mL) were labeled with 1 μM carboxyfluorescein succinimidyl ester (CFSE) Cell Division Tracker Kit (BioLegend) for 5 minutes at 37°C prior to quenching on ice for 5 minutes with 20 mL cold complete media. CFSE-labeled cells were mixed with 1 μL of nanoshuttles (n3D Biosciences, Houston, TX, USA) per 10,000 cells. These cells were incubated overnight at 37°C/5% CO_2. The next day, cells were magnetized for 30 minutes and plated at 2.5×10^5 cells per well of a 6-well plate with a 2-mL final volume. Cells were remagnetized for 30 minutes before the magnet was removed. The plate was placed in a Nano Dock Station for the desired time. Data images were recorded every hour by using an iPod and a magnifying glass on top of the plate, and analysis was performed using the National Institutes of Health ImageJ Software (imagej.nih.gov/ij/; provided in the public domain) with the Color Thresholding tool (color threshold and brightness were kept constant across all images). Following 48 hours, spheroids were fixed with 4% paraformaldehyde for 4 hours at RT and then washed with PBS (magnet was placed under plate during washes to maintain spheroid). We added 500 μL of 0.01% Triton X-100 for 15 minutes at RT. Blocking proceeded for 1 hour and was replaced by primary antibody (anti-PDGFRβ, sc-432, 1:100) and incubated overnight at 4°C. Alexa Fluor 647 donkey anti-rabbit IgG (catalog no. A31573; Invitrogen, Carlsbad, CA, USA; 1:100) secondary antibody was added and incubated for 2 hours at RT, followed by adequate washing. Samples were allowed to air dry for 1 hour before being imaged on a Nikon C1 confocal microscope (Melville, NY, USA).

RNA Isolation. RNA was extracted from Rb cell lines or PDX eye cross-sections with the Qiagen RNeasy Mini Kit (Valencia, CA, USA) according to manufacturer's instructions and our previously described protocols.[26,28,29] Rb cells were lysed and homogenized prior to the addition of chloroform. The upper, colorless phase underwent a DNase digestion and a series of alcohol precipitations prior to elution through a spin column. PDX tissues from the eye cross-section were lysed and homogenized, followed by the addition of deparaffinization solution, DNase digestion, and alcohol precipitation. RNA concentration was measured on a Nanodrop spectrophotometer.

cDNA Synthesis. The SuperScript VILO cDNA Synthesis Kit (Life Technologies, Grand Island, NY, USA) was used to synthesize cDNA as previously described.[26,28,29]

Preamplification of Material. The synthesized cDNA was preamplified with TaqMan PreAmp Master Mix. Gene expression assays (Thermo Scientific) included the following genes: *PDGFRA* (Hs00998018_m1), *PDGFRB* (Hs01019589_m1), *PDGFA* (Hs00234994_m1), *PDGFB* (Hs_00966522_m1), *MDM2* (Hs00540450_m1), *MDM4* (Hs00910358_m1), *VEGFA* (Hs00900055_m1), *FLT1* (*aka* VEGFR2, Hs01052961_m1), and *HPRT1* (Hs02800695_m1). Preamplified cDNA was maintained at -20°C until ready for use.

qPCR Analysis. A final 10-μL mixture of the preamplified cDNA, gene expression assays, nuclease-free water, and TaqMan Universal Master Mix were loaded into each well. Plates were processed via Roche LightCycler 480, and the results were analyzed according to the comparative ΔC_T method as describe before.[26,28,29]

siRNA Transfections. Y79 cells were plated overnight in 6-well plates at a final density of 3.0×10^5 cells per well in 2 mL Rb media (without antibiotics), following manufacturer's guidelines. Lyophilized *PDGFRB* siRNA duplex (sc-29942) was diluted in nuclease-free water to a final concentration of 10 μM, following manufacturer's instructions. A total of 0.6 μg of *PDGFRB* siRNA was diluted in 100 μL of siRNA transfection medium (Santa Cruz Biotechnology, Inc.) per well (solution A). In parallel, 6 μL of siRNA transfection reagent was added into 100 μL siRNA transfection medium (solution B) per well. Solution A and solution B were combined and incubated at RT for 30 minutes. Meanwhile, Y79 cells were harvested, washed in transfection medium and resuspended in 800 μL of siRNA transfection medium per well, following the addition of solution A and B. Cells were incubated for 6 hours at 37°C/ 5% CO_2. At this point, 1 mL of RPMI/20% fetal bovine serum was added, and cells were incubated for 18 hours prior to performing functional assays. As a control, we used a scramble sequence that is known to not target any specific oligonucleotides.

Quantification and Statistical Analysis. Data were analyzed using Prism 6 for Mac OS X (GraphPad Software, Inc., La Jolla, CA, USA). All bar graphs are expressed as mean ± SD or ± SEM (as indicated), with $P < 0.05$ considered statistically significant, as we have previously described.[23] Data sets were compared where appropriate by paired Student's *t* test or by the Holm-Sidak method, with alpha = 5.0%.

RESULTS

Expression of the PDGFR Signaling Network in Rb Tumors and Cell Lines

We investigated the nonphosphorylated and the phosphorylated (p-PDGFRβ) expression of PDGFRβ in primary human Rb samples from enucleated eyes of Rb patients with advanced intraocular disease with vitreous seeds. Our representative results from a cohort of 15 different samples (Figs. 1A–D) demonstrated an abundant p-PDGFRβ, shown by intensity of labeling, compared with the nonphosphorylated form. We measured abundant expression of the p-PDGFRβ (Figs. 1E, 1F) compared with the nonphosphorylated PDGFRβ in vitreous seeds. The human orthotopic xenograft for Rb has been already established as a comparable model to Rb disease. Using this system, we investigated the expression of PDGFRβ in samples from PDX. As shown in Figures 1G and 1H, there is less expression of the nonphosphorylated PDGFRβ compared with the p-PDGFRβ. Taken together, we observed activity of the PDGFRβ signaling network in vivo.

We examined the fold change of the two known PDGFRs *PDGFRA* and *PDGFRB* and their respective ligands *PDGFA* and *PDGFB* relative to the expression of the *HPRT1* in a cohort of nine different paraffin-embedded tissue samples from PDX in Figure 1I. The fold change of *PDGFRB* expression was higher than *PDGFRA*. *PDGFB* mRNA also measured a higher fold change compared with that of *PDGFA* in the PDX samples.

Y79 is considered a metastatic and aggressive cell line, whereas Weri-1 is considered the nonmetastatic Rb model.[30] Y79 measured a higher expression of *PDGFRB* compared with the *PDGFRA* mRNA (Fig. 1J, left). In contrast, Weri-1 Rb cells measured similar *PDGFRA* and *PDGFRB* mRNA expression
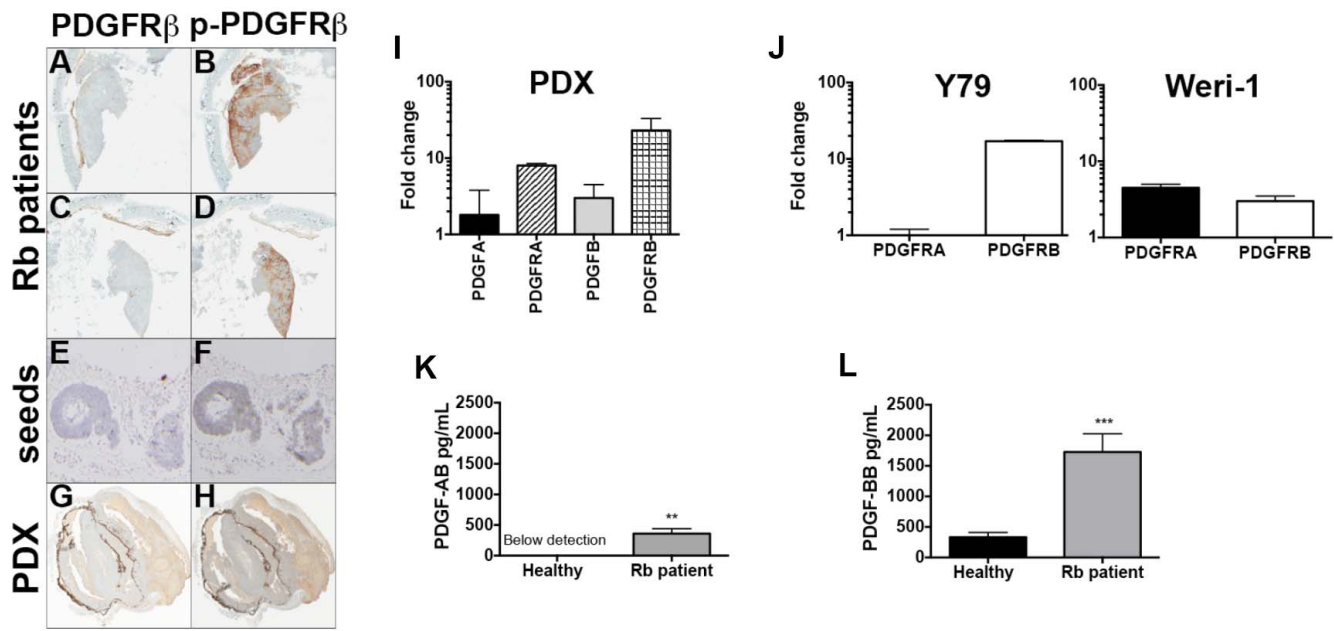
FIGURE 1. Expression of the active and nonactive forms of PDGFRβ in Rb. (**A–D**) Representative images of immunohistochemic staining for expression of nonphosphorylated PDGFRβ and p-PDGFRβ (active) from a cohort of 15 enucleated eyes of Rb patients. Images taken at 20×. (**E, F**) Representative image of immunohistochemical results of PDGFRβ in vitreous seeds. Images taken at 40×. (**G, H**) Images from PDX. Images taken at 20×. (**I**) qPCR analysis of mRNA from PDX for key members of PDGF signaling pathway. Results are represented as mean ± SEM fold change of the target gene over *HPRT1*, the housekeeping gene. (**J**) mRNA expression of both *PDGFRA* and *PDGFRB* in both Rb cell lines Y79 and Weri-Rb-1. Results are represented as mean ± SEM fold change of the target gene over *HPRT1*, the housekeeping gene. (**K, L**) Levels of PDGF-AB (**K**) and PDGF-BB (**L**) in vitreous samples from healthy controls vitreous compared to those of Rb patients by ELISA analyses. $n = 9$ in PDX mRNA analyses with 4 replicates per sample; $n = 4$ for Y79 and Weri-1 mRNA analyses with 4 replicates per sample; $n = 6$ in ELISA analyses done in triplicates. All results represent mean ± SEM; **$P = 0.0010$; ***$P = 0.00051$.

(Fig. 1J, right). Because vitreous seeds are considered an aggressive phenotype, we focused the rest of the in vitro studies on Y79 Rb cells.

To investigate the presence and abundance of PDGF proteins that signal through PDGFRβ in the vitreous microenvironment, we collected vitreous samples from eyes of Rb patients that underwent primary enucleation and compared the protein levels with those of healthy controls. We discovered PDGF-AB (Fig. 1K) to be more abundant in the Rb samples compared with those of healthy controls (**$P = 0.0010$). Similarly, PDGF-BB levels were higher in the Rb samples compared with healthy controls (***$P = 0.00051$). The levels of PDGF-BB in the Rb samples were >5-fold higher than the healthy controls (Fig. 1L). Our work reveals higher levels of active PDGFRβ as well as high levels of the receptor's ligands in Rb samples compared with healthy controls.

Pharmacologic Disruption of PDGFRβ Signaling Reduced Rb Proliferation, Invasion, and Increased Cell Death

We used IM, which selectively inhibits the tyrosine kinase activity of the PDGFRβ protein tyrosine kinase,[31,32] to disrupt the PDGF-PDGFRβ signaling pathway and investigate the role(s) it may play in Rb. We previously determined the most efficacious dose at inhibiting cellular proliferation was 10 μM (data not shown). The disruption of the PDGFRβ signaling pathway was confirmed by Western blotting (Fig. 2A). To mimic the physiology of the disease in the vitreous microenvironment, we added recombinant human PDGF (rhPDGF) to cell cultures. We measured increased levels of PDGFRβ activity when rhPDGF was added (*$P = 0.0073$). In contrast, there was a striking reduction of PDGFRβ activity when cells were

treated with IM (**$P = 0.0046$) or rhPDGF + IM (**$P = 0.0015$) compared with rhPDGF. Next, we quantified the percentage of Y79 PDGFRβ$^+$ cells by flow cytometry analysis and found a significant reduction of Y79 PDGFRβ$^+$ after 48 hours of treatment with IM compared with untreated (**$P = 0.0019$) and rhPDGF-treated cells (**$P = 0.0024$), as shown in Figure 2B, left. Representative histograms showing the percentage of PDGFRβ$^+$ Y79 cells are shown in Figure 2B, right. We measured cell viability by the MTS cellular proliferation assay. The results showed a significant increase in proliferation over time in the presence of rhPDGF, illustrating a potential mitogenic role. This mitogenic effect was inhibited by IM (Fig. 2C; *$P = 0.02$, **$P = 0.003$, **$P = 0.0016$, ***$P < 0.0005$). We then investigated if inhibition of PDGFRβ could increase cell death (Fig. 2D) by flow cytometry analysis of apoptotic (annexin V$^+$PI$^+$) cells. At the time of setting up the cell cultures, we measured cell death of Y79 cells to obtain the baseline levels. We measured cell death by colabeling of annexin V and PI and found about 3% cell death (Fig. 2D, right). There was an increase in cell death in IM and rhPDGF + IM compared with untreated and rhPDGF (**$P = 0.0021$, **$P = 0.0033$). These results illustrated the role of the PDGFRβ signaling in Rb cell growth and death.

We measured the invasive potential of Y79 cells by culturing them in well inserts coated with basement membrane through use of a colorimetric assay (Fig. 2E) and by quantitation of cells per field (Fig. 2F). There was a reduction in the colorimetric measurements of IM and rhPDGF + IM-treated cells that crossed the membrane (*$P = 0.0304$, **$P = 0.0070$) compared to those untreated and treated with rhPDGF. This data was confirmed with the quantitative analysis. IM-treated (*$P = 0.0357$; **$P = 0.0061$) and rhPDGF + IM-treated (*$P = 0.0118$) cells showed less invasion compared with untreated and rhPDGF cells. Representative images of cells in each condition are shown in Figure 2G.
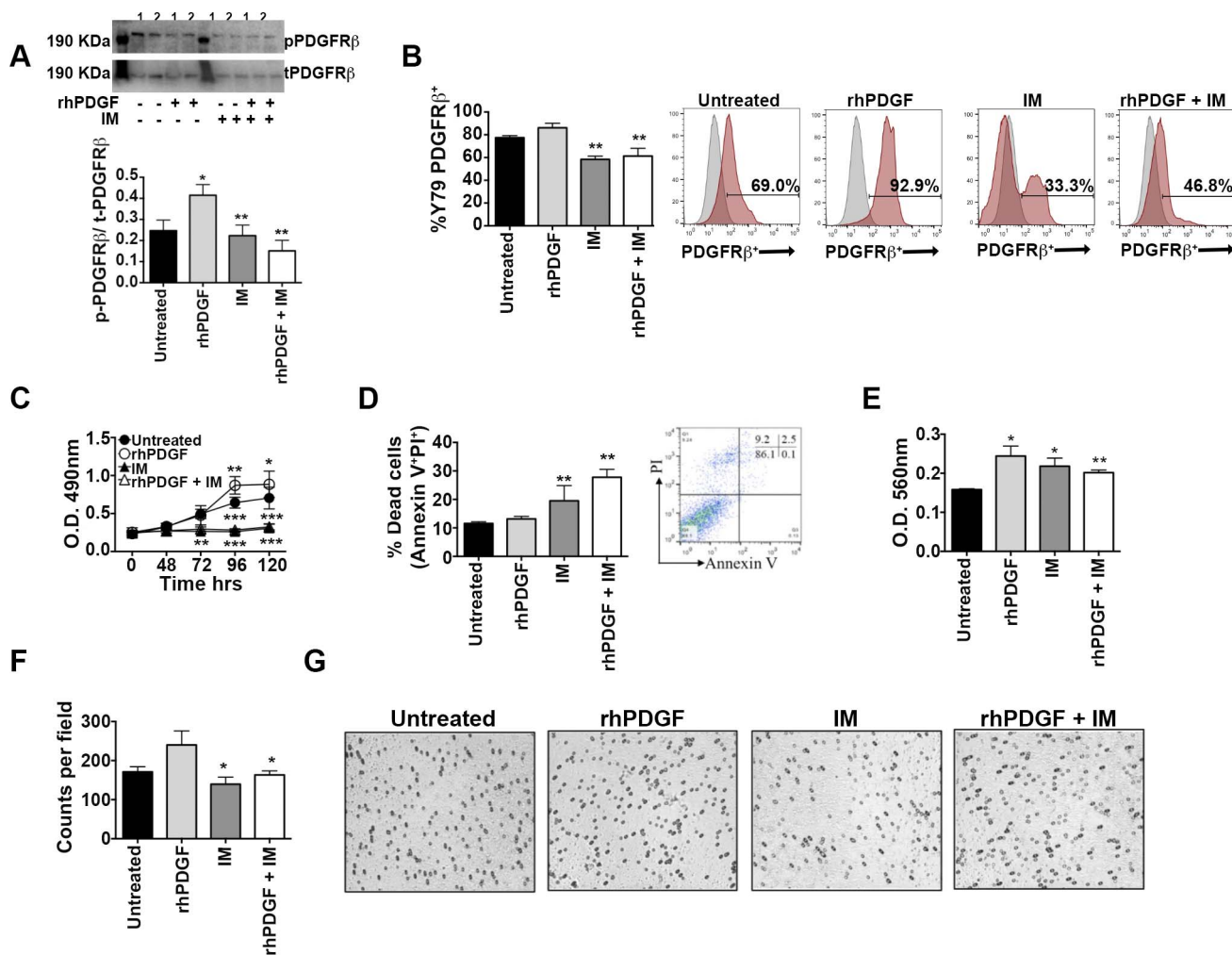
FIGURE 2. PDGFRβ signaling plays a role in proliferation, survival, and invasiveness of Rb cells. Y79 cells were cultured in the presence or absence of either PDGF-BB (10 ng/mL) and/or the PDGFRβ inhibitor IM (10 μM). (**A**) Western blot analyses of the activity of the PDGFRβ by measurement of the ratio of phosphorylated-PDGFRβ to total PDGFRβ. *$P = 0.0073$; IM, **$P = 0.0046$; rhPDGF + IM, **$P = 0.0015$. (**B**) Flow cytometry analyses showing the percentage of Y79 cells that express PDGFRβ. IM, **$P = 0.0019$; rhPDGF + IM, **$P = 0.0024$. (**C**) Assessment of Y79 cellular proliferation over time in the presence of either PDGF-BB or IM by using the concentrations described above. *$P = 0.02$; **$P = 0.003$; ***$P < 0.0005$. (**D**, *left*) The percentage cells undergoing apoptosis was measured by annexin V and PI labeling using flow cytometry. Dead cells displayed an annexin V$^+$PI$^+$ phenotype. (**D**, *right*) Evaluation of cell viability by annexin V$^+$PI$^+$ of Y79 Rb cells at 0 hours. IM compared with untreated, **$P = 0.0021$; rhPDGF + IM, **$P = 0.0033$, (**E–G**) Reduction in invasive capacity of Y79 cells after IM treatment on basement membrane-coated inserts. (**E**) Optic density measurements of invasive cells; rhPDGF, *$P = 0.0402$; IM, *$P = 0.0304$; **$P = 0.0070$; (**F**) total counts per field; and (**G**) representative images of fields counted $n = 3$ and 3 replicates per sample. Images taken at 10×; IM compared with untreated, *$P = 0.0357$ and compared with rhPDGF, **$P = 0.0061$; rhPDGF + IM compared with rhPDGF, *$P = 0.011$ All results represent mean ± SEM.

Disruption of PDGFRβ Targets the AKT and NF-κB Signaling Cascades

AKT and NF-κB signaling, which are linked to antiapoptotic mechanisms, have not been studied within the PDGFRβ pathway in Rb. Qualitative PCR analysis in Figure 3A demonstrated downregulation of *MDM2* mRNA after disruption of the PDGFRβ pathway compared with rhPDGF-treated cells relative to untreated cell cultures by using *HPRT1* as housekeeping gene. A similar effect was measured when *MDM4* mRNA (Fig. 3B) was tested. As shown in Figure 3C, MDM2 signaling is impaired in IM-treated (*$P = 0.0275$) and rhPDGF + IM-treated (**$P = 0.0011$) cells compared with the levels of untreated and rhPDGF. We investigated if the reduction in cell proliferation is AKT-dependent. A small, albeit significant (*$P = 0.0054$), difference was found in AKT signaling in rhPDGF + IM-treated cells (Fig. 3D).

After examination of MDM2 and AKT, both involved in cell survival pathways, we investigated the mechanisms by which PDGFRβ controls cell death in Rb. Figure 3E reveals Y79 cells treated with IM and rhPDGF + IM have a significant reduction in BCL-2 levels compared with untreated and rhPDGF by Western blot analyses (**$P = 0.001$; ***$P = 0.0002$). We sought to test the levels of cleaved caspase-3 by ELISA to investigate if the BCL-2 reduction was concomitant to an increase in cleaved caspase-3 (Fig. 3F). IM-treated cells showed a significant increase in cleaved caspase-3 (*$P = 0.007$) compared with the rest of the cell culture conditions.

Our next investigation aimed to evaluate if PDGFRβ signaling could exert an inhibitory effect in VEGF-VEGFR2 signaling, which is expressed in Rb.[26,33,34] We confirmed the expression of *VEGFA* mRNA in Y79 cells and in the PDX model of Rb (Figs. 3G, 3H). Additional qPCR analyses revealed no significant difference in *VEGFA* and *VEGFR2* mRNA expression after disruption of the PDGFRβ signaling (Figs. 3I, 3J). Despite
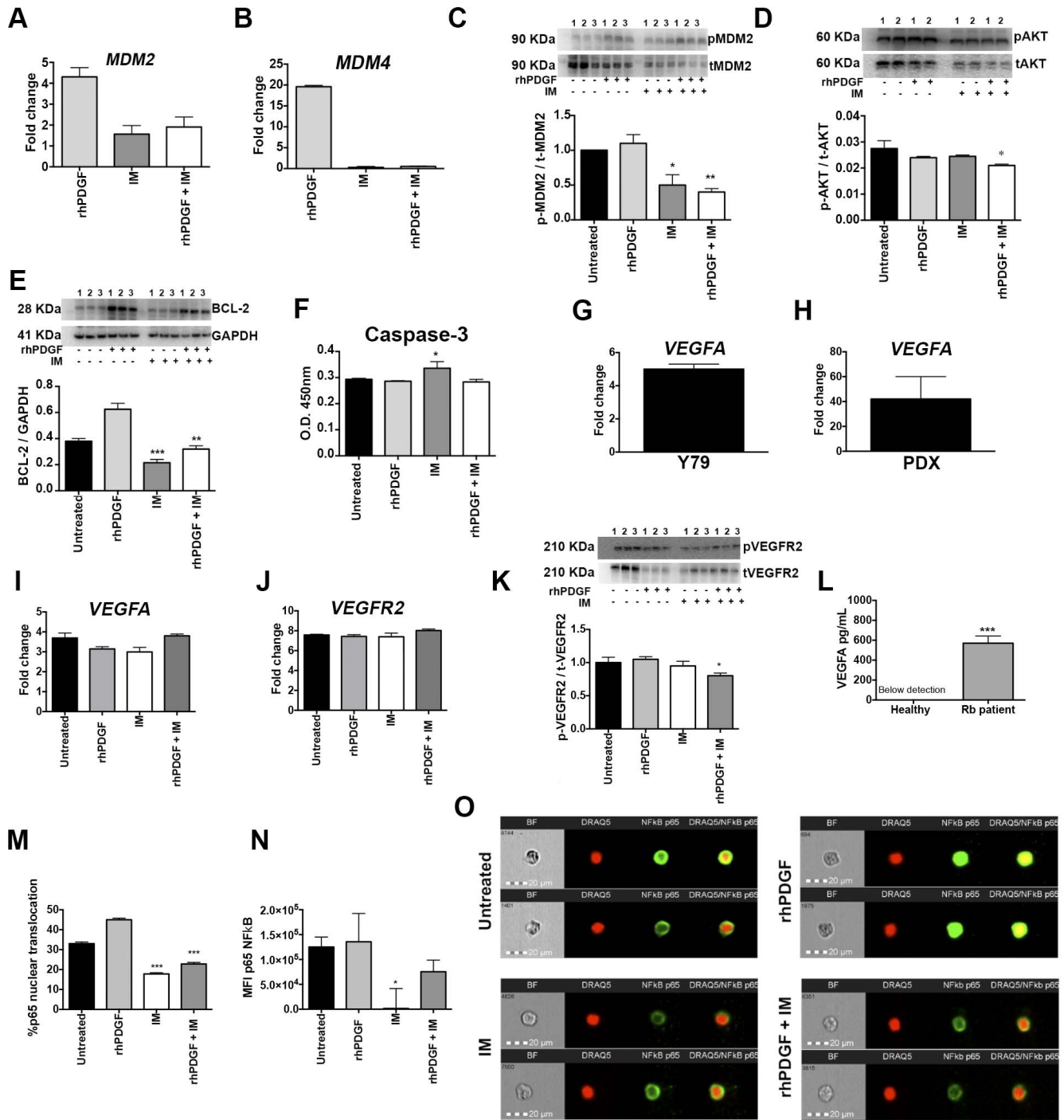
FIGURE 3. PDGF-PDGFRβ signaling regulates key downstream signaling mediators. qPCR analyses on mRNA levels of (**A**) *MDM2* and (**B**) *MDM4* relative to untreated Y79 cells under the cell culture conditions described above. *HPRT1* used as housekeeping gene. Western blot analyses (**C**) of MDM2 activity and (**D**) AKT activity after disruption of the PDGFRβ signaling cascade. IM, *$P = 0.0275$; rhPDGF + IM, **$P = 0.0011$; AKT, *$P = 0.0054$. Evaluation of the antiapoptotic mediator (**E**) BCL-2 by Western blot (**$P = 0.001$ and ***$P = 0.0002$); and the proapoptotic cleaved (active) capsase-3 by ELISA (**F**), *$P = 0.007$. (**G–L**) Downregulation of the VEGFR signaling when PDGFRβ is inhibited. (**G**) *VEGFA* mRNA levels were measured by qPCR analysis in both Y79 cells and (**H**) PDX samples. (**I**) Both *VEGFA* and (**J**) *VEGFR2* mRNA levels were measured across respective treatments as well as (**K**) Western blot analyses of VEGFR2 activity; *$P = 0.0191$. (**L**) Measurement of VEGFA levels in a cohort of vitreous samples from healthy controls compared to vitreous of Rb patients. ****$P = 0.0001$. (**M–O**) Assessment of the NF-κB signaling. Representing images of Y79 cells (**M**) labeled and analyzed for nuclear (labeled with DRAQ5) translocation of the p65 subunit of NF-κB (AlexaFluor 488 conjugated), ***$P < 0.001$ (**N**) the percentage of treated Y79 cells with nuclear localization of the p65 subunit and *$P = 0.0271$ (**O**) the expression (or MFI) of the p65 subunit using an Amnis FlowSight Imaging Cytometer. Experiments from **A–G** and **I–K** were done with $n = 3$ and each sample done in triplicates. Experiment from **H**, $n = 9$ and each sample done in replicates of 4. $n = 6$ in ELISA analyses done in triplicates. Experiments from **M–O** tested 10,000 cells per condition. All results represent mean ± SEM.
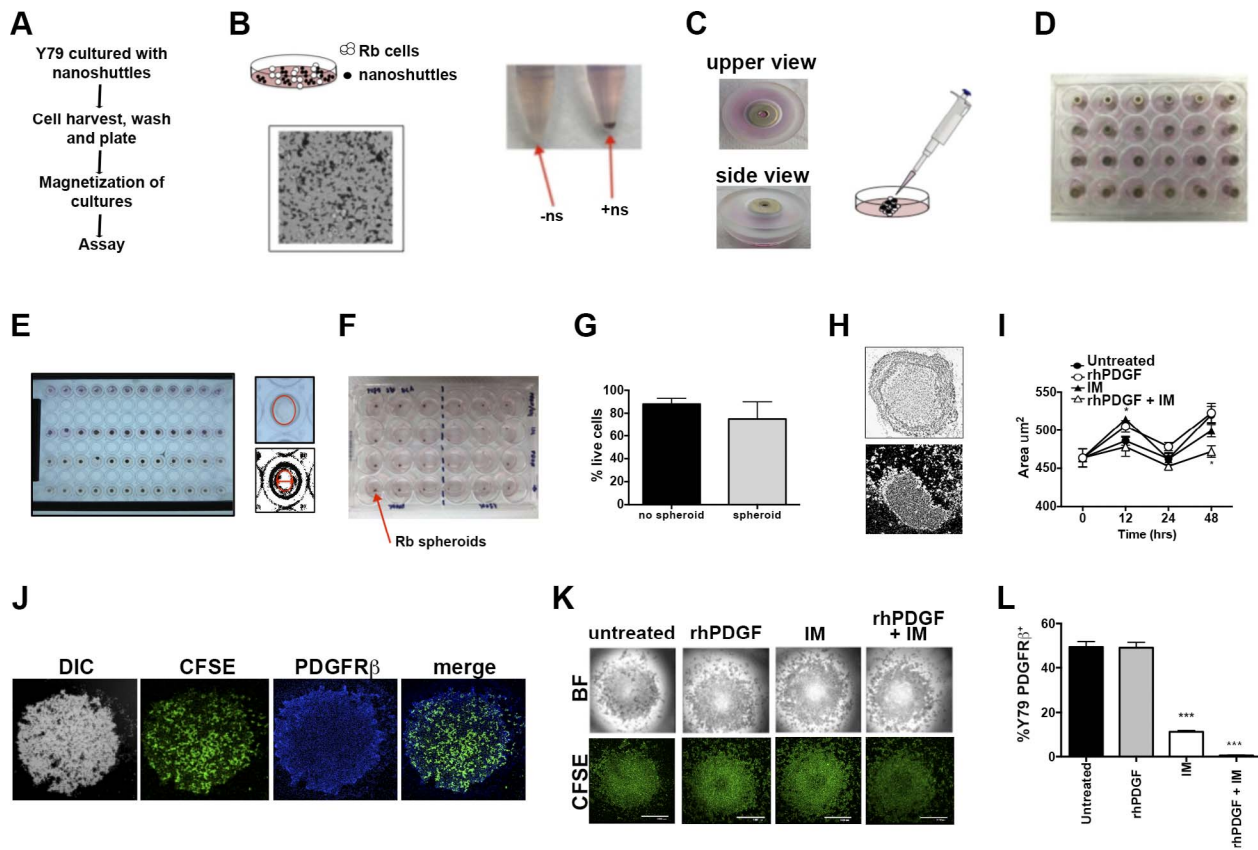
FIGURE 4. Disruption of the PDGFRβ signaling reduces three-dimension tumor spheroid size. (**A–F**) Using commercially available magnetic nanoshuttles, Y79 cells were combined with nanoshuttles (**B**). The cells were magnetized to form 3D tumor spheroids (**C**). Aggregates were disrupted and plated with a magnet specific for the assay (**D**). After completion of the assay, the plate was analyzed using the ImageJ software (**E**). At this point, the spheroids are visible to the naked eye (**F**). (**G**) Trypan blue exclusion was used to measure cell viability in samples with spheroid formation versus nonspheroid. (**H**, *upper*) Comparison of an ex vivo vitreous seed to (**H**, *lower*) a representative 3D tumor spheroid. (**I**) Plotted graph showing measurements of Rb spheroid area over time. *$P = 0.011$ (**J**, **K**) CFSE-labeled Rb spheroids were assessed morphologically 48 hours after culture. (**L**) CFSE-labeled Rb spheroids were disrupted by pipetting and labeled with anti-PDGFRβ. Labeled cells were evaluated by flow cytometry using a ZE5 Cell Analyzer. ***$P = 0.0001$. All results in **G**, **I**, and **L** represent mean ± SEM. In experiments **J** and **K**, minimums of 3 wells of spheroids were generated per culture condition.

no changes at the transcriptional level, there was a reduction in VEGFR2 signaling after treatment with IM (*$P = 0.0191$) compared with the controls, as shown in Figure 3K. These results suggest IM treatment could impact the abundance of VEGF protein in the vitreous microenvironment, which is shown in Figure 3L to be higher in Rb samples compared with healthy controls (***$P = 0.0001$). Taken together, these results demonstrated that targeting of PDGFRβ signaling impairs VEGFR2 signaling.

The disruption of PDGFRβ signaling via IM showed this pathway plays a role in Rb tumor cell survival via AKT. We hypothesized whether the suppression of Y79 survival may occur via a crosstalk between AKT and NF-κB. To address this, we used imaging flow cytometry to measure the nuclear translocation of the NF-κB p65 subunit (Figs. 3M–O). Quantitative analysis showed a distinct reduction in the percentage of cells showing p65 nuclear translocation (Fig. 3M) after IM treatment (***$P < 0.001$) compared with the untreated and rhPDGF controls. Along with a reduction on the percentage of cells showing p65 nuclear translocation, we measured an overall reduction in the p65 protein by measurement of the MFI (Fig. 3N) in the presence of IM (*$P = 0.0271$) compared with the controls. Representative images of the p65 nuclear localization analyses are shown in Figure 3O. Colocalization of p65 (green) to the nucleus (red) is depicted in yellow. Collectively, our work supports our

hypothesis that the PDGFRβ plays an essential role in Rb cell survival and death via AKT and NF-κB.

Reduction of Rb Spheroids by IM in a 3D Cell Culture Model of Rb Vitreous Seeds

There is a lack of in vitro models for Rb vitreous seeds. We adapted our in vitro 3D cell culture system to recreate Rb seeds in a vitreous-like microenvironment for an in-depth study. Schematics of the procedure are shown in Figures 4A–F. Rb cells are mixed with nanoshuttles (Fig. 4B) between 5 to 12 hours at 37°C/5% CO_2. These nanoshuttles are composed of poly-L-lysine, iron, and gold. Multiple aggregates or clusters of cells are found within the cell cultures. Cells are magnetized using a magnet, as depicted in Figure 4C. As "seeds" are generated by magnetic levitation, the aggregates are disrupted and plated. An additional magnet, which varies by type of assay, is applied for 30 minutes (Fig. 4D). Using the 3D system, we are able to generate a spheroid that forms one large mass visible to the naked eye (Figs. 4E, 3F). Quantitative analysis of live cells by trypan blue exclusion, shown in Figure 4G, revealed no difference ($P = 0.430$) in the viability of cells after overnight culture. We compared light microscopy images of the Rb spheroids to Rb seeds and found similar morphology (Fig. 4H). We then measured the area of the spheroids over time after treatment with IM using ImageJ software and
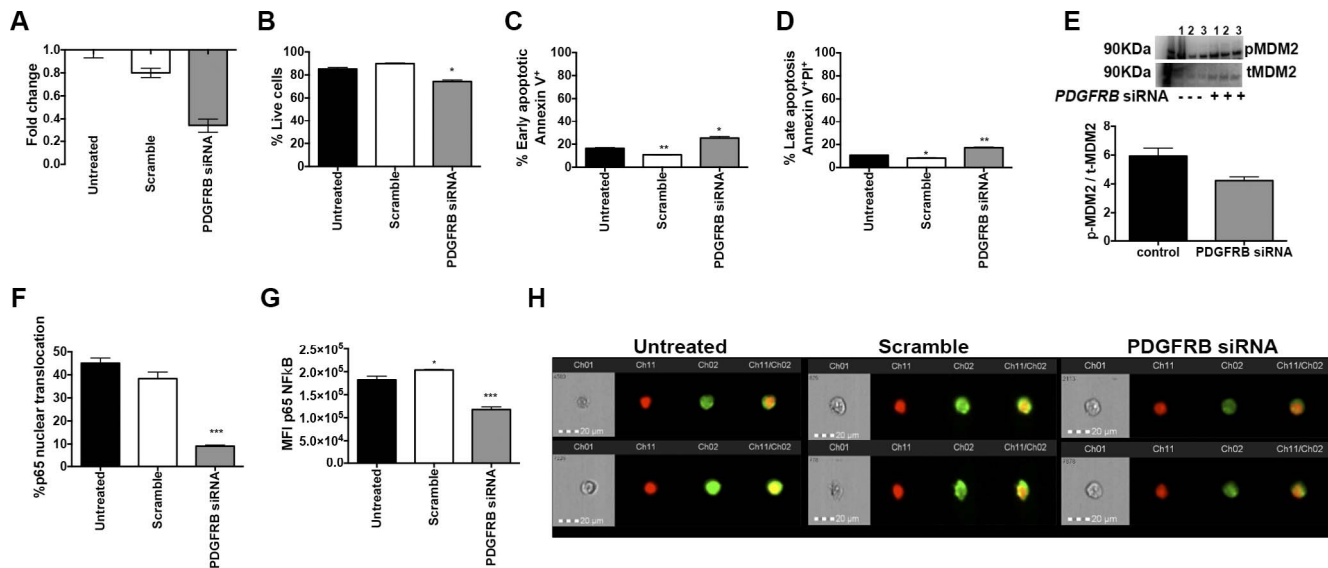
FIGURE 5. Confirmation of PDGFRβ-specific effects in Rb cells by *PDGFRB* siRNA. *PDGFRB* gene expression in Y79 was targeted using commercially available siRNA. (**A**) qPCR analyses confirmed effective knockdown of *PDGFRB* mRNA in siRNA-transfected samples compared to nonspecific oligonucleotides (scramble) and untreated cells. (**B–D**) The percentages of viable and apoptotic cells were determined by flow cytometry analysis using (**B**) the annexin V⁻PI⁻ phenotype for live cells; *$P = 0.019$ (**C**) the percentage of early apoptotic (annexin V⁺); *$P = 0.0107$; **$P = 0.0052$ and (**D**) late apoptotic (annexin V⁺PI⁺) cells; *$P = 0.0120$; **$P = 0.0029$. (**E**) Western blot analyses were done to measure activity levels of MDM2 after transfection of *PDGFRB* siRNA. (**F–H**) Using the Amnis FlowSight Imaging Cytometer, untreated, scramble, or *PDGFRB* siRNA-transfected Y79 cells were labeled and analyzed for (**F**) the percentage of p65 nuclear translocation; ***$P < 0.0005$ and (**G**) the expression (MFI) of the p65 subunit. (**H**) Representative images in each condition. Experiments from **F–H** evaluated 10,000 cells per condition. All results represent mean ± SEM.

discovered a significant reduction in the area of spheroids 48 hours after rhPDGF + IM treatment (*$P = 0.011$; Fig. 4I).

Y79 cells were labeled with CFSE to fluorescently visualize the cells. In Figure 4J, we observed PDGFRβ was localized in the outer edges of the spheroid. In addition, we observed the center of the spheroid to have fewer cells than the rest of the spheroid (Fig. 4K, shown 48 hours) when CFSE⁺ Rb spheroids were cultured over time. The size of the translucent center is larger in those spheroids treated with IM (both IM and rhPDGF + IM) compared with the untreated and rhPDGF groups, suggesting death. We confirmed our flow cytometry findings (Fig. 2B) of a reduction in the percentage of PDGFRβ (***$P = 0.0001$) in IM-treated cells (Fig. 4L) by using flow cytometry analysis of disrupted 3D spheroids. Through the use of a 3D cell culture model, we generated Rb spheroids that showed a reduction in the spheroid area and reduction in the percentage of cells expressing PDGFRβ after treatment with IM.

Reduction in Cell Viability, MDM2 Signaling, and p65 Nuclear Translocation after PDGFR Knockdown by siRNA

To confirm if the reduction of cell viability was PDGFRβ-specific or an off-target effect of IM, we knocked down *PDGFRB* by siRNA technology. Figure 5A demonstrates *PDGFRB* mRNA knockdown after *PDGFRB* siRNA transfection compared with samples transduced with random nucleotides and untreated controls. To address levels of apoptosis, we labeled cells with annexin V and PI labeling as in Figure 2D. The analysis showed a reduction in the percentage of live (annexinV⁻PI⁻) cells in *PDGFRB* siRNA transfected cells compared with the controls (Fig. 5B; *$P = 0.019$). The percentage of early apoptotic cells (Fig. 5C; *$P = 0.0107$; **$P = 0.0052$) with a phenotype of annexin V⁺PI⁻ increased in *PDGFRB* siRNA transfected samples compared with untreated and scramble-treated cells. Similarly, the percentage of late

apoptotic cells (Fig. 5D; *$P = 0.0120$; **$P = 0.0029$), defined as annexin V⁺PI⁺, increased in *PDGFRB* siRNA-transfected cells compared with untreated and scramble-transfected cells. The percentage of annexin V⁺PI⁺ cells was higher in scramble-transfected cells compared with untreated cells. However, the magnitude of the increase in the percentage of late apoptotic cells in *PDGFRB* siRNA-transfected cells is larger than those of the scramble-treated group. As part of our investigation on the role of PDGFRβ in Rb cell survival and death, we measured MDM2 signaling in the siRNA transfections. Western blot results in Figure 5E demonstrated a reduction, albeit not significant ($P = 0.06$), in MDM2 signaling in *PDGFRB* siRNA-transfected cells compared with the control group.

To confirm if the reduction in the p65 subunit of NF-κB and in the nuclear translocation after pharmacologic disruption of PDGFRβ was a PDGFRβ-dependent effect, we compared these parameters in *PDGFRB* siRNA-transfected cells to scramble and untreated controls (Figs. 5F–H). The results revealed a marked reduction of the percentage of cells showing p65 nuclear translocation in the *PDGFRB* siRNA-transfected (***$P < 0.0005$) cells (Fig. 5F; *$P = 0.0051$) in addition to a reduction in the amount of p65 protein (Fig. 5G) compared with the control groups. Colocalization of p65 (green) to the nucleus (red) is shown in yellow in Figure 5H. Our *PDGFRB* siRNA transfection findings confirmed our results by using the pharmacologic inhibitor of PDGFRβ IM and support our hypothesis that the PDGFRβ plays an essential role in Rb cell survival and death via both MDM2 and NF-κB signaling.

DISCUSSION

A recent study by Sanft and colleagues[35] demonstrated the presence of the PDGFRβ in Rb samples by immunohistochemistry. Our study demonstrates increased activity of the PDFGRβ signaling network ex vivo in primary human Rb samples from

enucleated eyes with advanced intraocular disease with vitreous seeds. We demonstrated this stimulatory circuitry by the high expression of *PDGFB* mRNA in Rb tumor cells, the levels of active PDGFRβ signaling, and the abundance of the PDGFRβ ligands in the vitreous microenvironment of Rb patients.

We recapitulated these finding in vitro by using the Y79 Rb cell line, which is considered to be the aggressive model of the disease. The in vitro system allowed us to demonstrate the role of the PDGF-PDGFRβ signaling pathway in Rb by using the selective tyrosine kinase inhibitor IM. Our mechanistic studies measured reduction of cell viability and invasive potential after disruption of the PDGF-PDGFRβ by IM in Y79 cells. These events were associated with a reduction of antiapoptotic mechanisms in the cell, including downregulation of *MDM2* mRNA, as well as reduced signaling activity of MDM2, AKT, the p65 subunit of NF-κB, and BCL-2. In addition, VEGFR2 signaling after disruption of PDGFRβ signaling with IM was noted. We postulate PDGF-PDGFRβ signaling may help regulate VEGF production in the tumor microenvironment, which is abundant under pathologic conditions.

Current investigations using IM in cancer,[36] specifically in glioblastoma multiforme, suggest a clinically safe application in the pediatric population and penetration across the blood-brain barrier (BBB). The blood-retinal barrier is the ocular counterpart of the BBB. Emerging evidence shows IM is also capable of reducing neuroinflammation in autoimmune disorders and restores the integrity of the BBB in a rat model of MS.[37,38]

Our limited understanding of vitreous seeds and the vitreous microenvironment has precluded the advancement in the development of novel therapies to specifically address this aspect of Rb. We generated a novel 3D Rb cell culture system based on the magnetic levitation studies originally from Haisler and colleagues[39] to develop tumor seeds in vitro. When these spheroids were examined morphologically, they were similar to in vivo Rb vitreous seeds. Munier and colleagues[7] recently outlined the three main subtypes of vitreous seeding patterns; each subtype may indicate different biologic properties of disease and potential different responses to conventional therapy. Amram et al[40] recently described the histopathology associated with each subtype and concluded spheres to be the most aggressive subtype. We compared our in vitro spheroids to the morphologic characteristics described in Amram's studies and discovered similarities to the spheres subtype, specifically the translucent center with some spheroids exhibiting Rb cell detachment from the outer area. This validation of our in vitro 3D system supported further study of Rb spheroids.

In this investigation, we demonstrated preclinically that PDGF from both autocrine and paracrine sources signals through the PDGFRβ to sustain Rb growth in an avascular system, such as the vitreous. Targeting the PDGFRβ could increase the sensitivity of these tumor cells to current treatments, as current therapies have failed to address the reduced proliferative capacity and metabolism of these unique tumor seeds.

Acknowledgments

The authors thank Abigail Lepsch-Combs, William Evans, Benjamin Emery, and Rajashekhar Gangaraju for technical help; Elizabeth Stewart, Charlene Henry, and Alberto Pappo at SJCRH for provision of study materials; Monica Jablonski, Lawrence Pfeffer, and Anton Reiner for helpful discussions; and members of the Flow Cytometry Core Facility and the Molecular Resource Center at UTHSC for discussions.

Disclosure: **Z.K. Goldsmith**, None; **W. Coppess**, None; **A.S. Irvine**, None; **K. Yuan**, None; **S.R. Barsh**, None; **M.K. Ritter**, None; **M.W. McEwen**, None; **J. Flores-Otero**, None; **A. Garcia-Vargas**, None; **M. Martinez-Ferrer**, None; **R.C. Brennan**, None; **V.M. Morales-Tirado**, None; **M.W. Wilson**, None

References

1. Chantada GL, Sampor C, Bosaleh A, Solernou V, Fandino A, de Davila MT. Comparison of staging systems for extraocular retinoblastoma: analysis of 533 patients. *JAMA Ophthalmol*. 2013;131:1127–1134.

2. Gunduz K, Gunalp I, Yalcindag N, et al. Causes of chemoreduction failure in retinoblastoma and analysis of associated factors leading to eventual treatment with external beam radiotherapy and enucleation. *Ophthalmology*. 2004;111: 1917–1924.

3. Sastre X, Chantada GL, Doz F, et al. Proceedings of the consensus meetings from the International Retinoblastoma Staging Working Group on the pathology guidelines for the examination of enucleated eyes and evaluation of prognostic risk factors in retinoblastoma. *Arch Pathol Lab Med*. 2009; 133:1199–1202.

4. Shields CL, Douglass AM, Beggache M, Say EA, Shields JA. Intravitreous chemotherapy for active vitreous seeding from retinoblastoma: outcomes after 192 consecutive injections. The 2015 Howard Naquin lecture. *Retina*. 2016;36:1184–1190.

5. Aman J, van Bezu J, Damanafshan A, et al. Effective treatment of edema and endothelial barrier dysfunction with imatinib. *Circulation*. 2012;126:2728–2738.

6. Shields CL, Honavar SG, Shields JA, Demirci H, Meadows AT, Naduvilath TJ. Factors predictive of recurrence of retinal tumors, vitreous seeds, and subretinal seeds following chemoreduction for retinoblastoma. *Arch Ophthalmol*. 2002;120:460–464.

7. Munier FL. Classification and management of seeds in retinoblastoma. Ellsworth Lecture Ghent August 24th 2013. *Ophthalmic Genet*. 2014;35:193–207.

8. Manjandavida FP, Honavar SG, Reddy VA, Khanna R. Management and outcome of retinoblastoma with vitreous seeds. *Ophthalmology*. 2014;121:517–524.

9. Dai Y, Wu Z, Sheng H, Zhang Z, Yu M, Zhang Q. Identification of inflammatory mediators in patients with rhegmatogenous retinal detachment associated with choroidal detachment. *Molecular Vis*. 2015;21:417–427.

10. Monteiro JP, Santos FM, Rocha AS, et al. Vitreous humor in the pathologic scope: insights from proteomic approaches. *Proteomics Clin Appl*. 2015;9:187–202.

11. Pollreisz A, Funk M, Breitwieser FP, et al. Quantitative proteomics of aqueous and vitreous fluid from patients with idiopathic epiretinal membranes. *Exp Eye Res*. 2013;108:48–58.

12. Angi M, Kalirai H, Coupland SE, Damato BE, Semeraro F, Romano MR. Proteomic analyses of the vitreous humour. *Mediators Inflamm*. 2012;2012:148039.

13. Freyberger H, Brocker M, Yakut H, et al. Increased levels of platelet-derived growth factor in vitreous fluid of patients

with proliferative diabetic retinopathy. *Exp Clin Endocrinol Diabetes*. 2000;108:106–109.

14. Morescalchi F, Duse S, Gambicorti E, Romano MR, Costagliola C, Semeraro F. Proliferative vitreoretinopathy after eye injuries: an overexpression of growth factors and cytokines leading to a retinal keloid. *Mediators Inflamm*. 2013;2013: 269787.

15. McAuley AK, Sanfilippo PG, Hewitt AW, et al. Vitreous biomarkers in diabetic retinopathy: a systematic review and meta-analysis. *J Diabetes Complications*. 2014;28:419–425.

16. Dai C, Celestino JC, Okada Y, Louis DN, Fuller GN, Holland EC. PDGF autocrine stimulation dedifferentiates cultured astrocytes and induces oligodendrogliomas and oligoastrocytomas from neural progenitors and astrocytes in vivo. *Genes Dev*. 2001;15:1913–1925.

17. Dong J, Grunstein J, Tejada M, et al. VEGF-null cells require PDGFR alpha signaling-mediated stromal fibroblast recruitment for tumorigenesis. *EMBO J*. 2004;23:2800–2810.

18. Guo P, Hu B, Gu W, et al. Platelet-derived growth factor-B enhances glioma angiogenesis by stimulating vascular endothelial growth factor expression in tumor endothelia and by promoting pericyte recruitment. *Am J Pathol*. 2003;162: 1083–1093.

19. Heldin CH. Targeting the PDGF signaling pathway in tumor treatment. *Cell Comm Signal*. 2013;11:97.

20. Xue Y, Lim S, Yang Y, et al. PDGF-BB modulates hematopoiesis and tumor angiogenesis by inducing erythropoietin production in stromal cells. *Nature Med*. 2011;18:100–110.

21. Reid TW, Albert DM, Rabson AS, et al. Characteristics of an established cell line of retinoblastoma. *J Natl Cancer Inst*. 1974;53:347–360.

22. McFall RC, Sery TW, Makadon M. Characterization of a new continuous cell line derived from a human retinoblastoma. *Cancer Res*. 1977;37:1003–1010.

23. Webb AH, Gao BT, Goldsmith ZK, et al. Inhibition of MMP-2 and MMP-9 decreases cellular migration, and angiogenesis in in vitro models of retinoblastoma. *BMC Cancer*. 2017;17:434.

24. McEvoy J, Flores-Otero J, Zhang J, et al. Coexpression of normally incompatible developmental pathways in retinoblastoma genesis. *Cancer Cell*. 2011;20:260–275.

25. Gao BT, Lee RP, Jiang Y, Steinle JJ, Morales-Tirado VM. Pioglitazone alters monocyte populations and stimulates recent thymic emigrants in the BBDZR/Wor type 2 diabetes rat model. *Diabetol Metab Syndr*. 2015;7:72.

26. Webb AH, Gao BT, Goldsmith ZK, et al. Inhibition of MMP-2 and MMP-9 decreases cellular migration, and angiogenesis in in vitro models of retinoblastoma. *BMC Cancer*. 2017;17:434.

27. Thakran S, Zhang Q, Morales-Tirado V, Steinle JJ. Pioglitazone restores IGFBP-3 levels through DNA PK in retinal endothelial cells cultured in hyperglycemic conditions. *Invest Ophthalmol Vis Sci*. 2015;56:177–184.

28. Chintalapudi SR, Djenderedjian L, Stiemke AB, Steinle JJ, Jablonski MM, Morales-Tirado VM. Isolation and molecular profiling of primary mouse retinal ganglion cells: comparison of phenotypes from healthy and glaucomatous retinas. *Front Aging Neurosci*. 2016;8:93.

29. Chintalapudi SR, Morales-Tirado VM, Williams RW, Jablonski MM. Multipronged approach to identify and validate a novel upstream regulator of Sncg in mouse retinal ganglion cells. *FEBS J*. 2016;283:678–693.

30. Chevez-Barrios P, Hurwitz MY, Louie K, et al. Metastatic and nonmetastatic models of retinoblastoma. *Am J Pathol*. 2000; 157:1405–1412.

31. Buchdunger E, Zimmermann J, Mett H, et al. Inhibition of the Abl protein-tyrosine kinase in vitro and in vivo by a 2-phenylaminopyrimidine derivative. *Cancer Res*. 1996;56:100–104.

32. Carroll M, Ohno-Jones S, Tamura S, et al. CGP 57148, a tyrosine kinase inhibitor, inhibits the growth of cells expressing BCR-ABL, TEL-ABL, and TEL-PDGFR fusion proteins. *Blood*. 1997;90:4947–4952.

33. Kvanta A, Steen B, Seregard S. Expression of vascular endothelial growth factor (VEGF) in retinoblastoma but not in posterior uveal melanoma. *Exp Eye Res*. 1996;63:511–518.

34. Arean C, Orellana ME, Abourbih D, Abreu C, Pifano I, Burnier MN Jr. Expression of vascular endothelial growth factor in retinoblastoma. *Arch Ophthalmol*. 2010;128:223–229.

35. Sanft DM, Worme MD, Rielo de Moura L, et al. Immunohistochemical analysis of PDGFR-alpha, PDGFR-beta and c-Abl in retinoblastoma: potential therapeutic targets. *Ophthalmic Res*. 2016;55:159–162.

36. Druker BJ, Talpaz M, Resta DJ, et al. Efficacy and safety of a specific inhibitor of the BCR-ABL tyrosine kinase in chronic myeloid leukemia. *N Engl J Med*. 2001;344:1031–1037.

37. Adzemovic MV, Zeitelhofer M, Eriksson U, Olsson T, Nilsson I. Imatinib ameliorates neuroinflammation in a rat model of multiple sclerosis by enhancing blood-brain barrier integrity and by modulating the peripheral immune response. *PLoS One*. 2013;8:e56586.

38. Crespo O, Kang SC, Daneman R, et al. Tyrosine kinase inhibitors ameliorate autoimmune encephalomyelitis in a mouse model of multiple sclerosis. *J Clin Immunol*. 2011;31: 1010–1020.

39. Haisler WL, Timm DM, Gage JA, Tseng H, Killian TC, Souza GR. Three-dimensional cell culturing by magnetic levitation. *Nat Protoc*. 2013;8:1940–1949.

40. Amram AL, Rico G, Kim JW, et al. Vitreous seeds in retinoblastoma: clinicopathologic classification and correlation. *Ophthalmology*. 2017;124:1540–1547.